

## **Trace space reconstruction data analysis**

P. Musumeci (*INFN/Roma1*), D. Filippetto (*INFN/LNF*)

### **Abstract**

In this note we summarize the trace space reconstruction algorithm and we apply it to the study of few typical experimental cases. The SPARC emittance measurement system uses the pepper-pot technique. Processing in a different way the information embedded in the beam images recorded for an emittance measurement, one can obtain a finite number of sample points for the beam distribution function in the transverse trace space. Using such finite ensemble of points we are able to reconstruct the beam distribution function with excellent accuracy. This allows to uncover the main features of the transverse trace space beyond the simple measured emittance value, and also to calculate the distribution moments offering an alternative strategy for filtering out of the data the beam halo and an interesting crosscheck of the rms emittance measure.

## 1 INTRODUCTION

The SPARC [1] emittance-meter measurement system is based on the traditional pepper-pot technique (schematized in Fig. 1) [2]. Because it is interesting to retrieve the beam quality over a wide range of beam sizes and divergences the measurement is performed using a multi-shot single slit scan, preferred over a single shot multislit mask which lacks of the required flexibility. The stability of the system is such that during the time of measure the beam conditions are stable. Of course shot-to-shot charge and pointing fluctuations contribute to blurring and uncertainty in the measurement. This is compensated by taking a sufficient number of beam images and by a detail error analysis that is the subject of another discussion which we refer the interested reader to. In the present paper we simply assume the beam stability sufficient to perform the single slit emittance measurement.

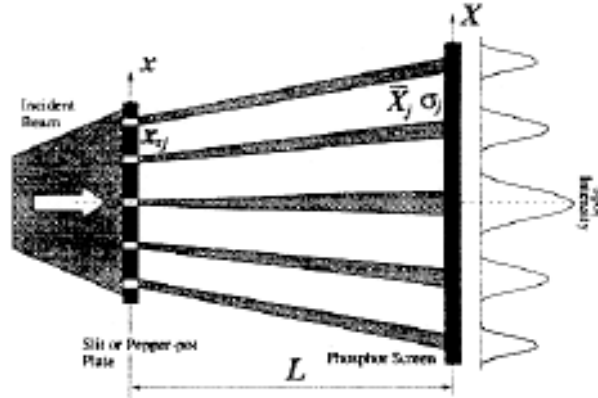


Figure 1. Pepper pot emittance measurement

In the SPARC emittance measure system, a  $50 \mu\text{m}$  slit was moved across the electron beam in  $N$  different positions, and the transmitted beamlet were propagated on a detection Yag fluorescent screen located at a distance  $L$  from the slit plane. The measurements which this paper refers to were commonly performed with  $N = 13$  and  $L = 300 \text{ mm}$  or  $400 \text{ mm}$ . Several images from the digital camera looking at the Yag screen were recorded for each slit position. Particular care has to be taken in choosing the number of beamlets to be used in the measurement and the extent of the scan across the beam transversely. The  $N = 13$  slit positions used in the SPARC emittance measurements are spaced one half of a beam rms size ( $\sigma_x / 2$ ) with positions ranging from  $-3 \sigma_x$  to  $+3 \sigma_x$ . This ensures that the entire beam is sampled in the measurement.

In order to calculate the rms emittance [3] one has extract from the images the information about the fraction of the beam transmitted through the slit, its mean divergence and its rms spread. From the determination of these values a well known numerical algorithm, which takes also in account the finite slit aperture, yields the full rms beam parameters  $\langle x^2 \rangle$ ,  $\langle x'^2 \rangle$  and  $\langle xx' \rangle$  and hence the emittance value.

Since for most applications, one is interested in the quality of the beam core, and can accept the existence of low charge low quality beam halos which either do not make it through a long transport or can always be scraped away, in the literature it is customary to

report and quote the 90 % rms emittance. We'll comply with this common practice by first (in the hardware data recording) taking the measurement of the whole beam emittance and then (in the analysis software) filtering out the 'outer' particles, recalculating the beam emittance for 90 % of the beam charge.

The emittance is a quantity built on the second moments of the distribution and it gives a good measure of the beam transverse quality but what this paper is aimed to point out, is that from a multishot single slit scan it is possible to extract information on the beam which largely exceeds the one encoded in the simple second order moments.

A particle beam is fully characterized once its distribution function  $f(x, p)$  which represents the particle density in phase space is known. We will exploit the fact that using the same data recorded during a multishot vertical (horizontal) slit scan it is possible to reconstruct with very good accuracy the projection of the beam distribution onto the horizontal (vertical) trace space  $f(x, x')$ . For a relativistic beam this is equivalent to the phase space distribution and the two terms are too often (even though not correctly) used interchangeably. It is also the only information available due to the fact that we measure angles and not momenta.

Other methods of phase space reconstruction such as transverse phase space tomography [4] are less feasible in the case one wants to study the dynamics of a low energy space charge dominated beam such is the one coming out of an RF photoinjector. On the other hand the latter is one of the cases where the beam dynamics is most interesting.

The method of trace space reconstruction we discuss in this note has many advantages, and this is at no extra cost since it uses the same data already taken for the rms emittance measurement. The reconstruction of the beam distribution function allows to develop a different strategy to filter out the beam halos which we discuss in the next section. By looking at the trace space reconstruction it is easier to understand the behavior of fundamental beam parameters like its emittance. The double peak divergence profiles observed during certain measurements at the SPARC photoinjector, which find no place in a second order moment description of the beam, are seen to represent different beam populations whose evolution can now be followed independently from one another without the need to describe the beam with only one set of Twiss parameters.

## 2 TRACE SPACE RECONSTRUCTION

A great deal of information on the beam phase space is hidden in the full beam images as it has already made clear when virtual experiment simulations were performed. Characteristic C-shaped slit images were explained as  $y-x'$  ( $x-y'$ ) correlations resulting from a cylindrically symmetric system which produces beam distributions depending on the cylindrical coordinate  $r = \sqrt{x^2 + y^2}$  and its divergence  $r'$ , but not separately from  $x-x'$  and  $y-y'$ . Limiting our analysis to a single plane (either vertical or horizontal) phase space, one projects the 2 dimensional image data onto the axis perpendicular to the slits and extracts for any given slit position an intensity profile  $G(X)$  which as we will see in the next few paragraphs is closely related to the beam divergence distribution.

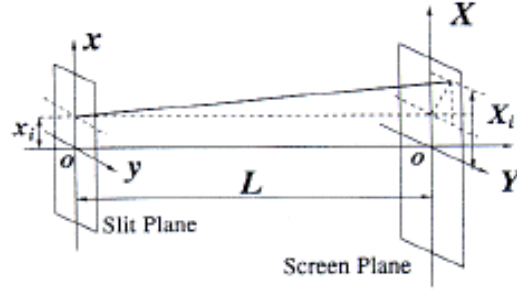


Figure 2. Divergence coordinate system

Assuming that only a drift transformation takes place between the slit and the screen, one can write the relationship giving the final coordinates  $(X, X')$  in terms of the initial ones  $(x, x')$ .

$$\begin{aligned} X &= x + x' L \\ X' &= x' \end{aligned}$$

The beamlet profile  $G(X)$  can be found taking the integral over  $x'$  of the beam distribution function

$$G(X) \propto \int f_{Yag}(X, X') dX' \quad (1)$$

where  $f_{Yag}(X, X')$  is the beam distribution function at the fluorescent Yag measurement screen. From the Liouville theorem we have

$$f_{Yag}(X, X') = f_{slit}(X - X' L, X') \quad (2)$$

and  $f_{slit}(x, x')$  is equal to the initial unknown beam distribution function  $f_{in}(x, x')$  over the slit aperture  $\Delta x$ , that is for  $x_0 - \Delta x/2 < x < x_0 + \Delta x/2$ , where  $x_0$  is the slit center coordinate and  $f_{slit}(x, x') = 0$  otherwise, since we assume that electrons which do not fall in the aperture do not reach the detection screen. In other words

$$f_{slit}(x, x') = \begin{cases} f_{in}(x, x') & \text{for } x_0 - \frac{\Delta x}{2} < x < x_0 + \frac{\Delta x}{2} \\ 0 & \text{otherwise} \end{cases}$$

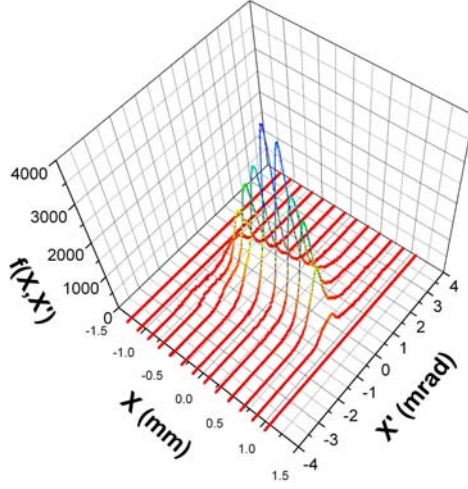
Inserting this into (1) and performing the change of variables  $Y = X - X' L$  in the integral we obtain

$$G(X) \propto \int_{x_0 - \Delta x/2}^{x_0 + \Delta x/2} f_{in}\left(Y, \frac{X - Y}{L}\right) dY \quad (3)$$

a sufficiently small  $\Delta x$  this quantity tends just to a line-out at position  $x_0$  so that there is a one-to-one correspondence between the beamlet profile  $G(X)$  and the divergence line-out at position  $x_0$  of the beam distribution function  $f(x, x')$ . That is

$$\lim_{\Delta x \rightarrow 0} G(X) \propto f_{in}(x_0, \frac{X-x_0}{L})$$

The reconstruction of the input phase space is based on collecting different line-outs placing the slit at  $N$  different positions across the electron beam. A three-dimensional plot representing the initial phase space distribution can in fact simply be obtained associating with each point of each profile an  $x$  coordinate given by the slit position ( $x_0$ ) and a  $x'$  coordinate equal to  $(X-x_0)/L$ . The height of the surface representing the beam distribution will be given by the profile value. An example of the result obtained plotting the points  $(x_i, x'_i, f_i)$  is given in Fig. 1.



In order to have a distribution centered around the trace-space origin ( $x = 0, x'=0$ ) we subtracted from positions and angles the coordinates of the centroid of the beam distribution.

$$x_i = x_i - \frac{\sum_i f_i x_i}{\sum_i f_i}$$

$$x'_i = x'_i - \frac{\sum_i f_i x'_i}{\sum_i f_i}$$

An interpolation procedure is then used to fill in between the line-outs and obtain a contour plot of the beam distribution function (see Fig. 4.). The interpolation procedure differs from common two dimensional function reconstruction algorithms since it uses the fact that in this particular reconstruction case the sample points are dense in one direction ( $x'$ ) and relatively sparse in the other ( $x$ ) as it is evident from Fig.3. The interpolation algorithm is tailored to fill in along the  $x$  direction the missing line-outs. Instead it maintains the same sampling rate (pixel size/ $L$ ) in the  $x'$  direction.

Clearly our analysis would benefit from taking a larger number of sample line-outs, that is moving the slit over a larger number of positions across the beam. The resolution in the  $x$  direction is in fact limited by the spacing of the slit positions. In order to keep into account the fact that the beam changes dramatically size over the region we are interested in measuring the transverse phase space quality, our choice was to keep constant the ratio of sampling rate to the beam rms size, by varying the distance between each slit position accordingly ( $\sim \sigma_x/2$ ).

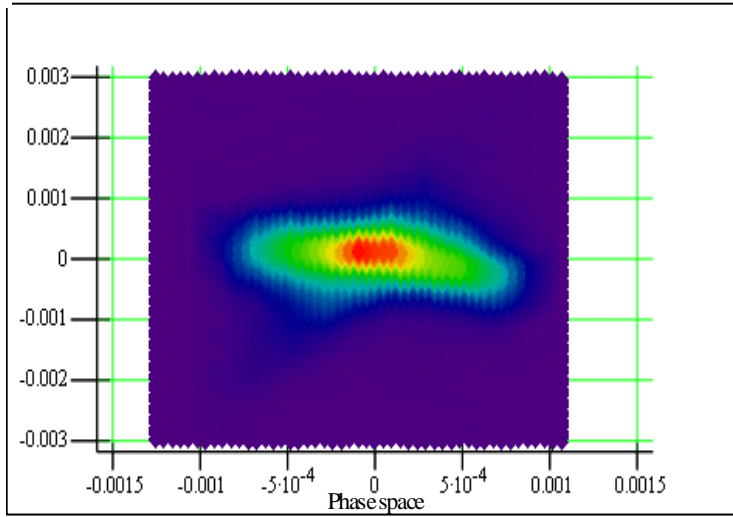


Figure 4. Contour plot of beam distribution

The resolution in the  $x'$  direction in principle could achieve a level set by the image acquisition optical system (pixel size/  $L$ ), but it is in fact greatly reduced by the convolution integral appearing in (3). Only for a vanishingly small aperture the profile  $G(X)$  really reproduces the divergence line-out. In practice, it is impossible to distinguish features in the beam distribution which have angles differing less than the slit aperture over the slit-screen distance. In our case, for a distance between the slit and the Yag screen of 0.4m, and a slit width of 50 microns the resolution of the phase space reconstruction in the  $x'$  direction is approximately  $\sim 0.125$  mrad. If one is interested in phase space reconstruction applications of the pepper-pot technique, in order to improve the resolution, it would be advisable to choose a slit width as small as possible. This choice on the other hand is limited by various factors, such as for example, the number of electrons transmitted which affects the signal to noise ratio of the image measurement.

Once the beam distribution function is known (at least in a well representative number of discrete points) one can of course calculate all the various moments, including the second order moments

$$\langle x^2 \rangle = \frac{\sum_i f_i x_i^2}{\sum_i f_i}$$

$$\langle x'^2 \rangle = \frac{\sum_i f_i x_i'^2}{\sum_i f_i}$$

$$\langle xx' \rangle = \frac{\sum_i f_i x_i x_i'}{\sum_i f_i}$$

where the sum is over all the distribution sample points. The emittance is then calculated with the usual formula  $\varepsilon = \sqrt{\langle x^2 \rangle \langle x'^2 \rangle - \langle xx' \rangle^2}$ .

### 3 FILTERING OUT THE BEAM HALOS

An important possibility that is offered from knowing the beam distribution function is to choose a different strategy for filtering out the beam halos.

As we discussed before, for most of electron accelerator applications it matters the quality of the beam core and beam users are often willing to accept that a small fraction of the beam does not meet the required specifications (beam halos). For this reason in comparing the quality of the beams from different machines, it is helpful to consider an halo-independent quantity such as the 90% rms emittance, which is just the rms emittance calculated using the corresponding fraction (90%) of the beam charge.

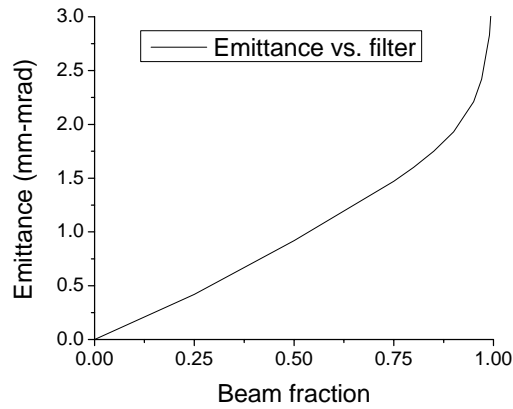


Figure 5. Calculated emittance vs. fraction of beam used in the second order moment sums.

Usually one neglects the ‘outer’ particles (larger excursions in the transverse coordinate  $x$ ) which have a relatively large weight in the second order moment sums. In the traditional pepper-pot algorithm this can easily done by setting a threshold for the minimum fraction of the beam transmitted through the slit at a given position in order to include (or not) the relative data in the second order moment summations. The fact that the beam emittance decreases by a percentage much larger than the fraction of the beam filtered out (see Fig.5) is an indirect confirmation of the halo nature of the scraped particles.

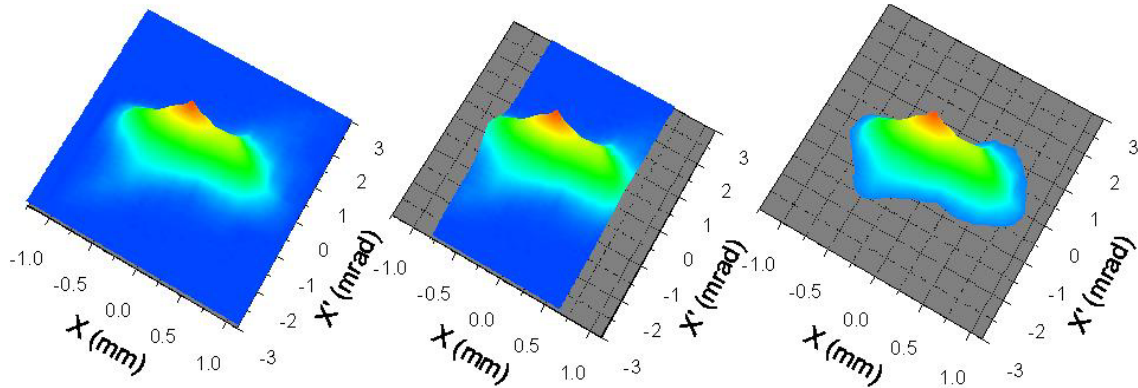


Figure 6. Trace space distribution a) not filtered, b) large offset particles filtered out, c) filtered in position and angles

In our case, after the full phase space distribution function has been reconstructed, it is possible to choose a different filtering criterium and to individuate the particles that are at the edge of the beam distribution in phase-space, not just in the coordinate space. In Fig. 6 it is clarified the difference of the approaches to the filtering problem. In the first case Fig. 6a, the particles with large  $x$  are filtered out until the charge considered is 90 % of the total charge. In the second case, Fig. 6b, we filter out particles with either large  $x$  or large  $x'$ , by setting a threshold on the beam distribution function values ( $f_i$ ) until the fraction of the beam considered and used in the emittance calculation is 90 % of the total charge.

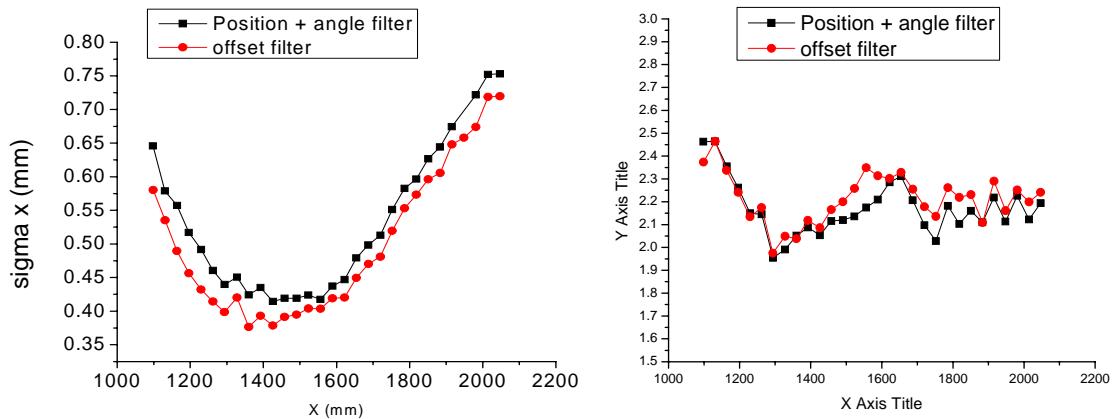


Figure 7. Comparison between different filtering strategy. Rms beam size (a) and emittance (b)

The result of the application of the two filters is exemplified in Fig. 7 for a longitudinal emittance scan extracted from the SPARC data set. In the traditional pepper-pot analysis

algorithm where one has the slit information, the 90 % rms beam size is smaller, since only particles with large transverse offset have been filtered out as opposed to the second case where also particles with large angles are neglected. The emittance on the other hand shows an opposite trend. Filtering out both in offset and angle results in a slightly (<5%) lower emittance number. The emittance behavior along  $z$  is unmodified.

Since practically the filtering is done with a scraper, it is only possible to make a selection for the beam core in the coordinate space. On the other hand, it depends on the optical transport system if the particles that have large transverse offset at the scraper and so will be scattered away are the same one that had large offsets at the emittance measurement plane. This dependence on the filtering procedure, which is typical of any emittance measurement, can be considered a systematic error on the measured value. It is important to note that while the uncertainty can be up to the 5 % level it is still much less than the statistical error due to the shot-to-shot beam fluctuations.

The really inestimable advantage of knowing the reconstructed phase space distribution is that it carries a lot more information than just its second order moments and it paves the way towards a novel detailed look and understanding of the beam dynamics.

As a preliminary example, let us show a glimpse of the unique measurements which can be done with the SPARC set-up. With the emittance-meter [5] in fact, it is possible to follow the evolution of a space charge dominated beam in its first meters of propagation after the RF gun. The electron beam dynamics in this region is characterized by emittance oscillations due to the linear correlations generated in the gun between longitudinal and transverse phase spaces.

In Fig. 7 we show the normalized 90 % rms emittance as a function of distance from the cathode. We also show seven representative phase spaces corresponding to seven different positions along  $z$  to illustrate how deep one can see some interesting features of the beam dynamics. A more detailed analysis and understanding of this data go beyond the scope of the present note and they will be the subject of further work.

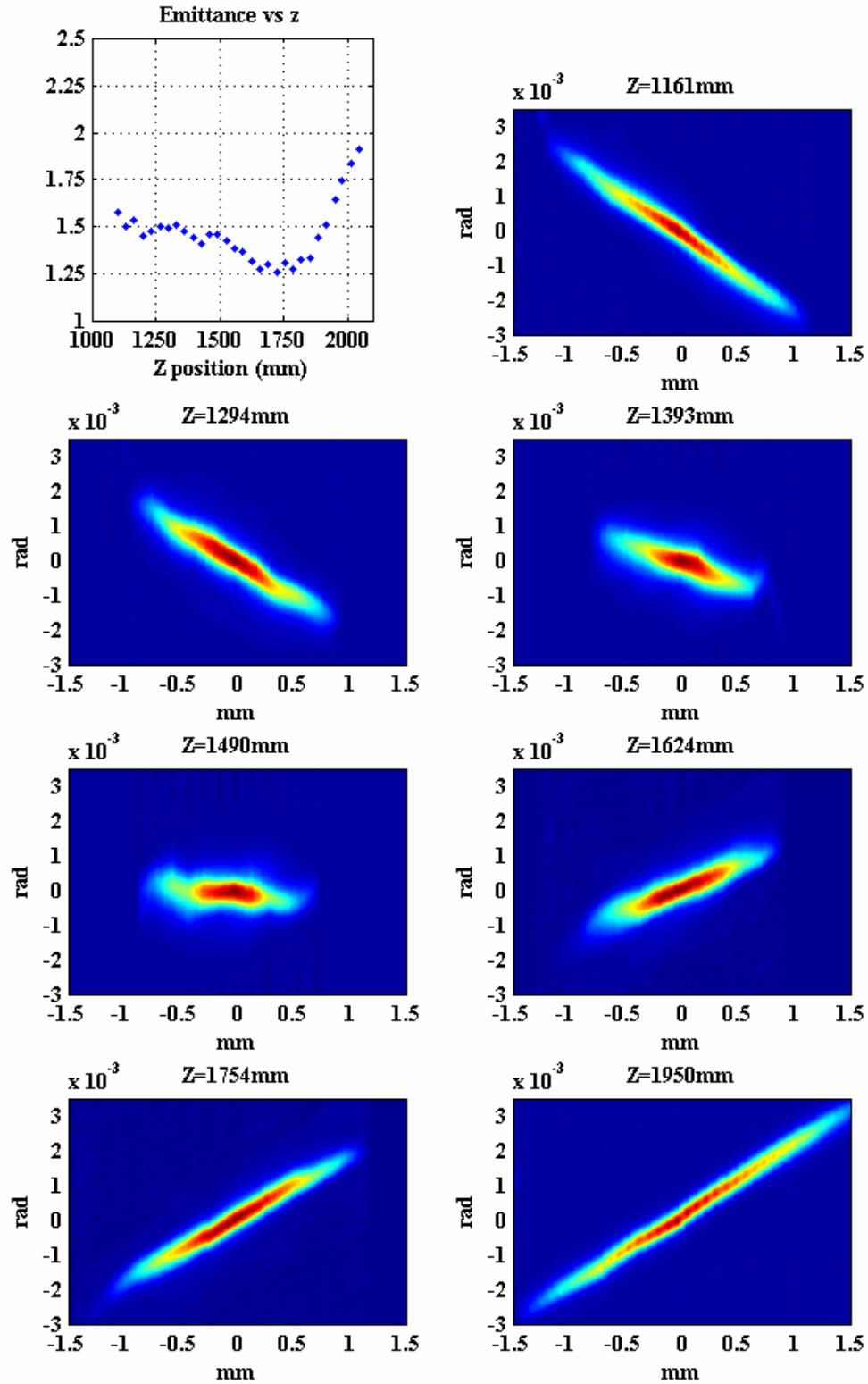


Figure 7. Trace space evolution for the gaussian beam scan of Dec. 3rd 2006

## 4 CONCLUSIONS

The trace space beam diagnostics presented in this note offers an important add-on to traditional beam characterization based on rms emittance and Twiss parameters. This study originates from the recognition that the large amount of data collected for a single slit-based emittance measurement carries more information about the beam distribution than just its second order moments.

The theoretical basis of the data analysis algorithm that reconstructs the beam density distribution in the  $x$ - $x'$  space is reviewed. An alternative strategy to filter out beam halos based on the two dimensional trace space distribution is presented. The emittance values found when filtering both in  $x$  and  $x'$  are only less than 5 % different than the ones obtained removing large offset particles.

A detailed investigation of the dynamics of low energy photoinjector beams conducted with this novel analysis tool could lead to a deeper understanding of the evolution of such systems. In theory, even more information could be found trying to extract x-y correlations from the collected images. On the other hand, if one is after such kind of correlations in the beam dynamics a pepper-pot based emittance measurement system is more appropriate than the slit-based one which is available on the emittance-meter.

Finally, these detailed measurements of the beam evolution offer a unique possibility to validate and benchmark simulation tools in order to design ultra low emittance beam sources for FEL and advanced accelerator applications.

## 5 REFERENCES

- [1] SPARC Project Team, *Technical Design Report for the SPARC Advanced Photoinjector*, <http://www.lnf.infn.it/acceleratori/sparc> (2004)
- [2] C. H. Wang, M. Clausen, Z. Kakucs, M. Zhang, *Proceedings of ICALEPS, 1999 Trieste, Italy* p. 284 (1999)
- [3] O. R. Sander, G. N. Minerbo, R. A. Jameson and D. D. Chamberlin, *Proc. Of the Linear Accelerator Conference 1979* (1979)
- [4] C. B. McKee, P. G. O'Shea, J.M.J. Madey, *Nuclear Instruments and Methods in Phys. Res. A*, **358**, 264 (1995)
- [5] L.Catani et al. "Design and characterization of a movable emittance meter for low-energy electron beams", *Review of scientific Instruments*, **77**, 093301 (2006)